ELSEVIER

Coastal Engineering 22 (1994) 311-339

COASTAL ENGINEERING

The modelling of wave action on and in coastal structures

M.R.A. van Gent

Hydraulic and Geotechnical Engineering Division, Department of Civil Engineering, Delft University of Technology, 2600 GA Delft, Netherlands

(Received 28 December 1992; accepted after revision 6 July 1993)

Abstract

Description of the wave action on and in coastal structures can lead to a prediction of flow properties and forces on elements of those structures. For permeable structures several aspects concerning the interaction between the external flow and the internal flow have to be described accurately to predict for instance velocities and run-up levels. The P.C.-model ODIFLOCS, developed at Delft University of Technology within the framework of the European MAST-Coastal Structures project, describes the wave motion on and in several types of structures. This structure can be an impermeable or a permeable structure. For instance dikes, breakwaters and submerged structures can be dealt with. The model is a one-dimensional model based on long wave equations. The program takes various phenomena into account such as reflection, permeability, infiltration, seepage, overtopping, varying roughness along the slope, linear and non-linear porous friction (Darcy- and turbulent friction), added mass, internal set-up and the disconnection of the free surface and the phreatic surface. Satisfactory results were obtained with modelling of run-up, surface elevations and velocities. Other applications show more possibilities of the model.

1. Introduction

The numerical model described in this paper is a model that simulates the wave action both on, and within coastal structures. In this numerical model ODIFLOCS, *O*ne *Di*mensional *Flo*w on and in *C*oastal *S*tructures, a hydraulic model is coupled to a porous flow model. For the hydraulic model long wave equations have been used. Kobayashi et al. (1987) showed that those equations can be applied successfully to describe the wave motion on impermeable structures. The numerical model described here uses adapted long wave equations for the porous flow model. The coupling of those two models requires some attention for aspects like for instance the disconnection of the free surface and the phreatic

0378-3839/94/$07.00
SSDI 0378-3839(93)E0030-M

surface. Those aspects will be discussed. Furthermore, verification with measurements of run-up and run-down levels, surface elevations and velocities will be discussed. A sensitivity analysis has also been performed. Applications where internal set-up and permeability are of importance are shown. The approach to obtain two-dimensional impressions of the flow field finalizes this paper.

2. Description of the hydraulic model

The hydraulic model, simulating the external flow, is similar to the model described by Kobayashi et al. (1987). This one-dimensional description of the flow includes hydrostatic pressures, the use of depth-averaged velocities (u), a description of the water volume with a single layer of water (h) varying in the x-direction and in time, and a simulation of a breaking wave like a bore. The following equations are used:

$$\frac{\partial hu}{\partial t}+\frac{\partial hu^2}{\partial x}=-gh\frac{\partial h}{\partial x}-gh\tan\theta-\frac{1}{2}fu|u|+qq_x$$

$$\frac{\partial h}{\partial t}+\frac{\partial hu}{\partial x}=q \quad (1)$$

In the first equation, the momentum equation, the influence of the pressure gradient as a result of the slope of the free surface and as a result of the slope of the bottom elevation (with angle θ) as well as the influence of the bottom friction (with coefficient f), are taken into account. The model for the external flow partially overlaps with the porous flow model. The q (m/s) stands for the flow between the external and internal flow per unit of length where the length is taken along the x-axis. This flow transports momentum from the external flow to the internal flow and visa versa which is represented by the term $q \cdot q_x$ where q_x is the x-component of the velocity of this interactive flow. The long wave equations are solved with an explicit second-order method (Lax-Wendroff), using a constant grid space and a constant time-step.

The slope of the structure is divided in a number of slope sections where for each slope section the angle of the slope and the friction coefficient, are taken constant. The friction coefficient f can be estimated using the empirical formula from Madsen and White (1975) for fully turbulent flow on a uniform sloping breakwater.

On the seaward boundary an incident wave is computed with either the Stokes second-order wave theory or the Cnoidal wave theory. This seaward boundary allows a reflected wave to leave the computational domain. This is calculated with the method of characteristics and allows water and momentum to leave the computational domain.

The boundary at the slope is based on work by Kobayashi et al. (1987) and is applied in the numerical model IBREAK. It uses a minimum water depth Δ at the wave front. If the depth in a certain computational point becomes smaller than Δ, this slope point is set dry. This point becomes the last wet point in the computation. In the approach by Kobayashi, this treatment has been applied only for the wave front (last wet point). In the model described here, at any point where the depth becomes smaller than Δ, that slope point is set

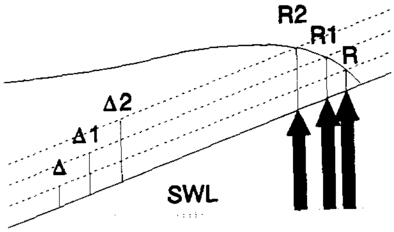

Fig. 1. Boundary at the slope.

dry. If a volume of water exists further upward the slope, the computation will proceed without this volume.

Alternative run-up levels R_i and run-down levels can be calculated using several levels Δ_i parallel to the slope. For such a level Δ_i, the slope is assumed to be dry in case the water-level is lower than this value (see also Fig. 1). Fig. 1 shows the level Δ which is the level that is actually used in the computation. The other values of Δ_i are levels to determine alternative run-up levels and have no influence on the computation itself. A good calibration of the model results in a prescription of the value Δ_i to be used for the actual run-up and run-down levels. Other values of Δ_i can show the sensitivity of the computed run-up and run-down levels to the choice of a certain Δ_i.

The model can compute overtopping. For the boundary at the slope in case of overtopping, a non-reflecting boundary is chosen. This makes the model also applicable for submerged structures. One-dimensional models are less accurate if for instance large changes in the slope elevation occur with respect to the used space step. Therefore, the model can not be applied on for instance overtopped vertical structures. However, a fully reflecting boundary has been implemented to deal with not-overtopped vertical (or partially vertical) structures. This makes the model also applicable for structures with vertical structures at the crest. However, the description of the surface elevation in a one-dimensional model requires that the wave action near such a vertical part is relatively calm.

3. Description of the coupled porous flow model

3.1. Adapted equations

Several aspects of the coupling will be described in detail in the next section. In this section, the adapted equations and the general lay-out of the model will be discussed.

The long wave equations used for the porous flow model have to be written with filter velocities instead of pore velocities. This means that the velocities u and q_x have to be replaced by respectively u/n and q_x/n where n is the porosity. The porosity is taken constant in the whole porous part. Conservation of mass requires that the flow q has to be replaced by q/n. Added mass is implemented in the momentum equation using the coefficient c_A. With $c=(1+c_A)/ng$, this coefficient c_A corresponds to the extended Forchheimer equation $I=au+bu|u|+c\partial u/\partial t$ where a, b and c are dimensional coefficients and I the hydraulic gradient. The linear- and non-linear friction terms are implemented as well. The coefficients

a, b and c are taken constant in time and space. The derivation of the equations for the porous part as used in the numerical model, is given by Van Gent (1992b). The equations can be written as follows:

$$(1+c_{\mathrm{A}})\frac{\partial hu}{\partial t}-c_{\mathrm{A}}u\frac{\partial h}{\partial t}+\frac{1}{n}\frac{\partial hu^2}{\partial x}=$$

$$-\mathrm{ng}\frac{\partial\frac{1}{2}h^2}{\partial x}-ngh\tan\theta_{\mathrm{c}}--ngh(au+bu|u|)-\frac{qq_x}{n}$$

$$\frac{\partial h}{\partial t}+\frac{1}{n}\frac{\partial hu}{\partial x}=-\frac{q}{n} \tag{2}$$

Expressions for a and b are prescribed by many authors. See for instance discussions by Hannoura and Barends (1981) and Van Gent (1992a). Here, the following are used:

$$a=\alpha\frac{(1-n)^2}{n^3}\frac{\nu}{gD^2}$$

$$b=\beta\frac{1-n}{n^3}\frac{1}{gD} \tag{3}$$

where D is a representative diameter of the particles, and ν is the kinematic viscosity. Although the non-dimensional parameters α and β depend on the gradation, aspect ratio, shape, the Reynolds number (Re) and the Keulegan-Carpenter number (KC), constant values have been used in the numerical model. Further study to determine these dependencies will be carried out.

3.2. General lay-out of the model

The porous part can be seen as a layer that partially overlaps with the hydraulic layer. The porous part of the model is sub-divided into several areas that are varying in size during the computation. The final equations depend slightly on the area in which they are applied because not all phenomena are present in the entire porous part.

The part of the porous medium that is overlapped by the hydraulic model is area P1 (see Fig. 2) in which the thickness of the porous layer h_{p} is time-independent. The pressure gradient in this area is caused by the slope of the free surface. The term $-ng\partial(\frac{1}{2}h^2)/\partial x$ describing the pressure gradient becomes: $-ngh_{\mathrm{p}}\,\partial(h_{\mathrm{h}}+h_{\mathrm{p}})/\partial x$ where h_{h} is the thickness of the hydraulic layer and h_{p} is the thickness of the porous layer. The part in which infiltration through a partially saturated area appears is area P2. In case the phreatic level reaches the slope, while no (external) layer of water is present there, seepage appears in this area. Both infiltration and seepage are assumed not to transport significant momentum in the x-direction. In area P2 the slope of the free surface has no direct influence on the water in the porous medium. In area P3 the terms with q and q_x are zero because no direct flow from, or towards the outer part, is present here.

The slope of the structure has already been discussed in the description of the hydraulic model. For the internal area an impermeable underlayer has to be described. This is done

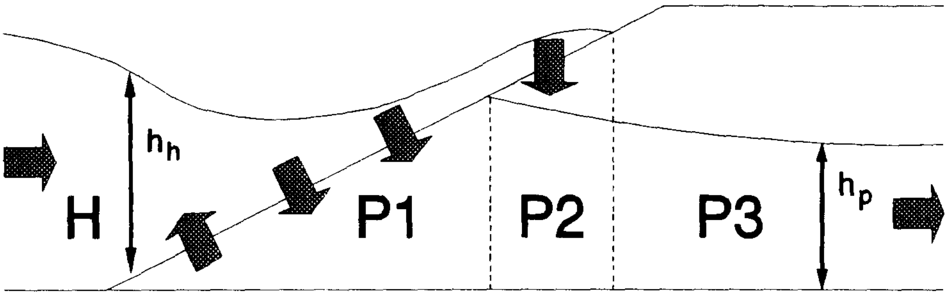

Fig. 2. Area's with different treatment.

in a similar way as for the slope sections. The impermeable underlayer can be horizontal, resulting in a homogeneous structure, or can be given a shape like an impermeable core. This core is again divided in several core sections with a constant angle of the slope for each section. This core can penetrate through the phreatic water-level. In this case the last point of the porous water-layer is treated in a similar way as for the last point of the external water-layer. The treatment of this internal boundary point is done in a more simple way to save computing time. In case overtopping of the impermeable core takes place (phreatic level higher than the crest of the core), a non-reflecting boundary is chosen at this internal boundary. At this boundary, the actual phreatic level converges towards a previously prescribed phreatic level, $h_{p(x=\infty)}$. For this value the surface elevation on the landward side has to be prescribed. In most cases, for this level the still water-level will be prescribed.

4. Aspects of the coupling

4.1. Basic idea of the coupling

In the numerical model, the coupling between the external flow and the internal flow is mainly determined by the pressures. The pressures caused by the variations in the free surface elevations, result in a flow (velocities) in the porous region underneath the hydraulic region (area P1 in Fig. 2). Continuity of mass gives the discharges of the interactive flow between the external part and the internal part (q in Eq. 2). The discharges are put as sources to the hydraulic region. Conservation of mass and conservation of momentum are served (terms with q in Eq. 1). The disconnection of the free surface and the phreatic surface leads to infiltration (flow from H to P2 in Fig. 2) or seepage (flow from P2 to H in Fig. 2).

The implementation of phenomena like infiltration and seepage is required to provide that the free surface and the phreatic surface can be uncoupled (discontinue surface). Those phenomena may have been implemented in a rather simple way. However, modelling of the motion of water on and in a structure with a continuous surface, would give an unrealistic coupling. Forcing the movement of the phreatic level so that it stays connected with the external free surface, causes disturbance of both the external and the internal motion.

4.2. *Maximum velocity at the phreatic surface*

The downward vertical velocity of the phreatic surface has a maximum. This is the result of the equilibrium of gravity and friction. If this maximum would be exceeded, the gradient in the pressures would be larger than one. This means that the water would flow quicker than the ''free seepage velocity'' which is not possible. The upward velocity has a maximum as well. This velocity is in the same order of magnitude as the maximum downward velocity. This aspect is implemented in the model HADEER, see Hölscher et al. (1988), although in that numerical model coefficients are added to change these maximum vertical velocities. The maximum upward velocity can be taken different from the maximum downward velocity. In the numerical model, the maximum vertical velocity is taken the same in both directions. In formula:

$$I = aw + bw|w| \leqslant 1$$

where I stands for the pressure gradient in the vertical direction and w for the vertical velocity. For w, $\partial h_p / \partial t$ is taken. The maximum vertical velocity of the phreatic surface can easily be solved from this equation. The exact maximum differs from this value because the flow does not have to be completely vertical at the phreatic surface.

4.3. *Flow between the models*

4.3.1. *Main interactive flow*

The flow q between the external flow in area H (see Fig. 2) and the internal flow in area P1 has a physical maximum. This is similar to the maximum vertical velocity at the phreatic line as described in the previous section. The difference, however, is that this velocity can be larger than the ''free seepage velocity'' because the pressure gradient (I) can be larger than unity. The exact pressure gradient in the vertical direction is unknown in a one-dimensional model because the pressures are assumed to be hydrostatic which is not completely true. Because the maximum of the flow q is depending on the maximum pressure gradient in the vertical direction, an assumption has to be made for the value of this maximum pressure gradient. A value of one is assumed in the model. However, it can be enlarged if desirable. This implies that a maximum entrance (and outward) velocity can be imposed.

4.3.2. *Infiltration*

In area P2 of Fig. 2, infiltration appears if the hydraulic surface appears above the phreatic surface with a ''dry'' area or partially saturated area in-between (see also Fig. 3). In area P2 the pressures of the hydraulic part have no direct influence on the porous part. The velocity of the infiltrated water is computed using the maximum seepage velocity as described in section 4.2. This velocity of the infiltrated water may differ from this maximum seepage velocity but it can be used as an approximation. This maximum seepage velocity is the recommended value for the velocity of the infiltrated water but in the model it is possible to multiply this recommended maximum seepage velocity with a coefficient. The recommended value for this coefficient is one. In the partially saturated zone the infiltrated water can be spread in the horizontal direction due to the influence of the stones. The infiltrated water does not flow through the partially saturated zone with a clear ''front''.

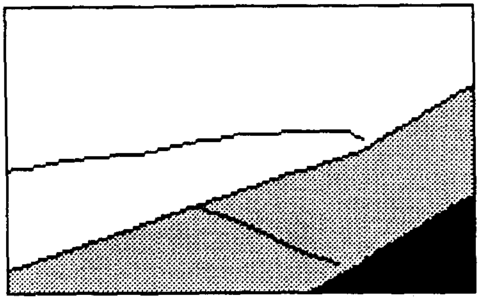

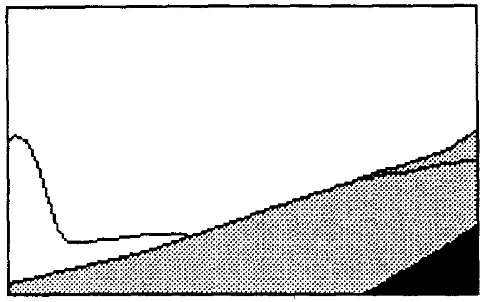

Fig. 3. Situation with infiltration.

Fig. 4. Situation with seepage.

The volume of the infiltrated water will not stay one volume but will be divided in smaller volumes. The infiltration is assumed to be vertical so no spreading caused by the porous medium is included. In the model, the infiltrated volume of water reaches the phreatic surface instantaneously.

4.3.3. Seepage

A different phenomenon, seepage, appears in area P2 (see Fig. 2) in case the phreatic surface reaches a "dry" slope. See also Fig. 4. The new phreatic surface is computed without the restriction that this surface has to stay inside the structure; if the new phreatic surface appears to be above the slope of the structure, the volume above this boundary (outside the structure) is assumed to be the flow outward the structure. The restriction concerning the maximum value of the velocity of the phreatic level results in a maximum value of the velocity of this seepage.

4.4. Internal porous boundary

The boundary point between area P1 and P2 (see Fig. 2) needs some special attention. The pressure gradient can be relatively large. The phreatic surface can fluctuate in this internal boundary point between two levels. See also Fig. 5. These levels are exactly in-between the slope elevation of the boundary grid point and the slope elevation of the neighbouring grid points. So, the phreatic level (h_p in Fig. 5) can fluctuate between the lower limit and the upper limit. If the phreatic level becomes lower than the lower limit, the internal boundary point is moved to the left. If the level becomes higher than the upper limit the boundary point is moved to the right.

5. Verification of run-up and run-down levels

5.1. Run-up on smooth impermeable structures

Run-up and run-down levels have been compared with measurements. First, a verification of run-up and run-down levels on an impermeable structure had to be performed to verify

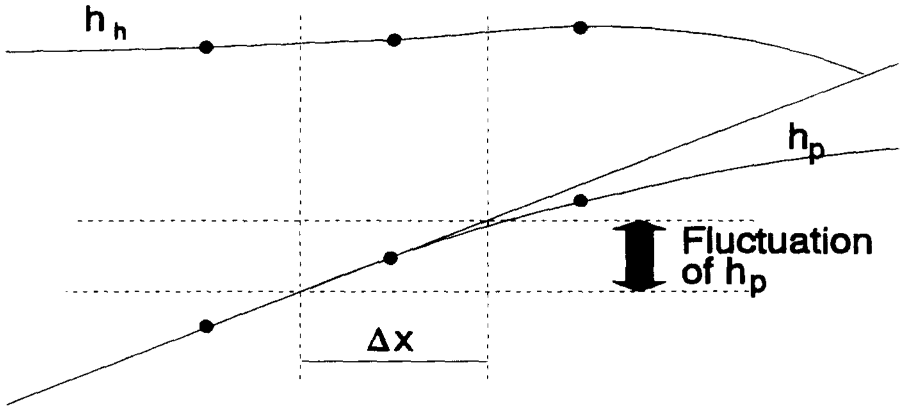

Fig. 5. Internal porous boundary.

the accuracy of the treatment of the boundary at the slope. With respect to the treatment of this boundary point, run-up on smooth slopes are the most difficult to describe with a numerical model because of the relatively large fluctuations on the slope. Therefore, verification on smooth slopes has been performed.

Measurements performed by Burger and Van der Meer (1983) in the Delta flume, have been used for verification of run-up and run-down levels. The run-up and run-down levels were measured visually. The waves were generated using reflection compensation. Regular waves were generated on a slope 1:3. The wave heights were roughly between 0.2 and 1.1 m.

The results of the comparison are summarized in Fig. 6. The non-dimensional run-up and run-down levels are printed as a function of the surf similarity parameter ξ_0. This figure shows that tests were done with plunging, collapsing and surging waves. The relations proposed by Van der Meer and Klein Breteler (1990), are shown in the figure as well. For the friction coefficient f, a value of 0.005 was used.

The figure shows that the numerical model gives the (measured) maximum for the transition from plunging waves to collapsing waves. The agreement between the measured and computed run-up levels is rather good. The computed run-down levels differ much more from the measured levels except for the range $2 < \xi_0 < 3$.

5.2. *Run-up on permeable structures*

The run-up and run-down levels for an impermeable structure are satisfactory as shown in the previous section. Run-up levels on a permeable slope have been verified using 49 tests, performed by Ahrens (1975), on uniform sloping structures. Tests with three slope angles were used: 1:2.5, 1:3.5 and 1:5. The stones (D_{EQ}) varied between 0.20 m and 0.34 m. Wave heights and wave periods varied between respectively 0.55–1.15 m and 2.8–11.3 s. The surf similarity parameters ξ_0 varied between 0.7 and 6.3. The depth in front of the structure was 4.58 m. For the friction coefficient f, the empirical formula from Madsen and White (1975) for fully rough turbulent flow on a uniform slope has been used:

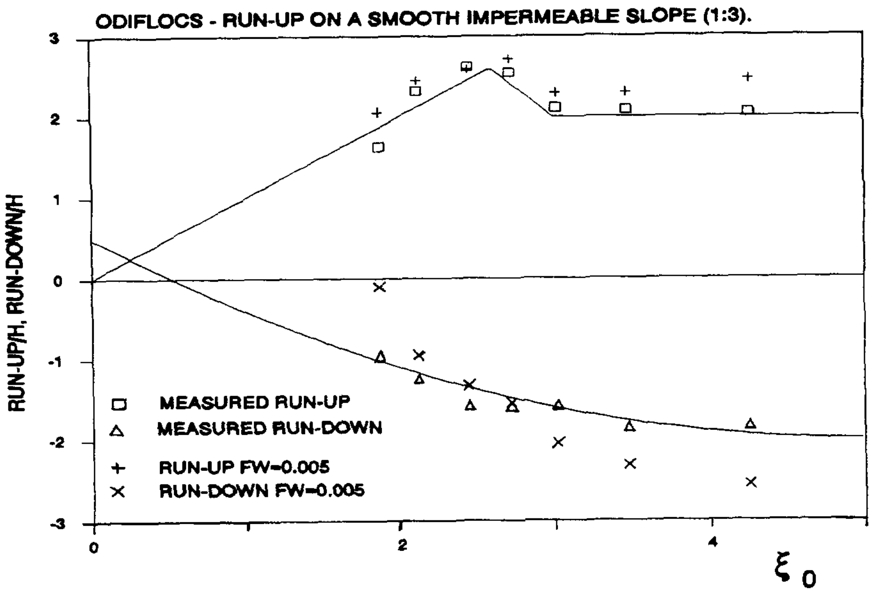

Fig. 6. Comparison with measured run-up and run-down levels.

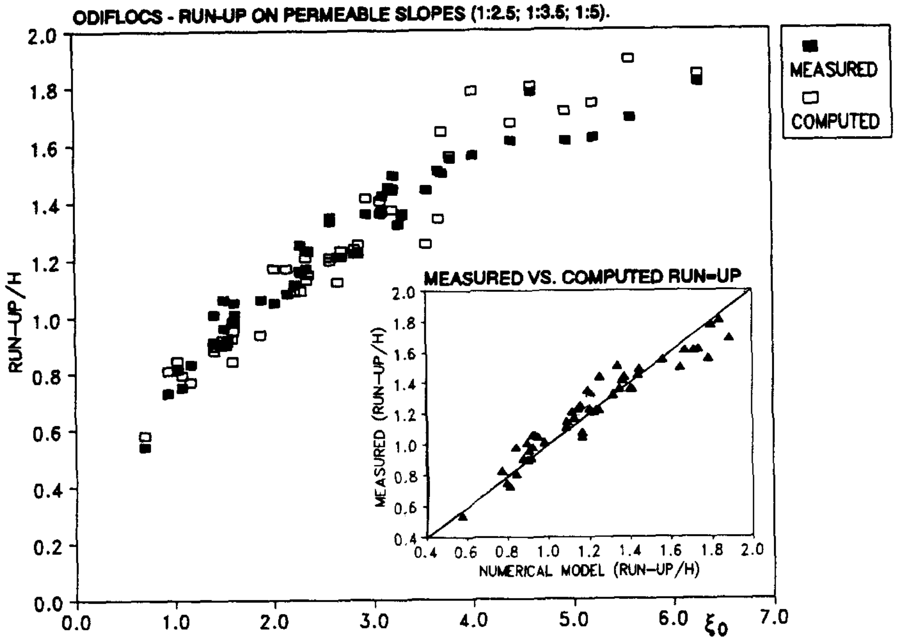

Fig. 7. Comparison between 49 measured and computed run-up levels.

$f=0.29\cdot(D/d_s)^{-0.5}\cdot(D/R\cot\alpha)^{0.7}$. For the maximum run-up level R the value 1.5 times the wave height was used as an approximation. The depth in front of the structure $d_s=4.58$ m was the same for all tests. The stone diameter D, the wave height and the angle of the slope α varied. The structure had a core of sand material. This has been implemented in the computations as an impermeable core. During the test, the porosity of the filter layer was estimated to be 0.40. This has been used in the computations. For the α and β respectively 2120 and 2.0 (see Eq. 3) have been used. Added mass has not been modelled.

The results are summarized in Fig. 7. The non-dimensional run-up levels R_u/H are shown as a function of the surf similarity parameter. The agreement is rather good. For the highest values of surf similarity parameter ($\xi>6$), the deviations increase. In general, one can conclude that the estimation of run-up levels on permeable slopes is satisfactory.

6. Verification of surface elevations

Measurements performed at the Norwegian Hydrotechnical Laboratory-Trondheim were used for verification. The measurements were done above the most gentle sloping part of a berm breakwater. See Fig. 8 and Tørum (1992) or Tørum and Van Gent (1992); η denotes the position where the surface elevation is measured.

The berm breakwater had a permeable core. The numerical model can deal with only one porous layer. For a berm breakwater with a core, the choice has to be made whether the breakwater will be modelled as a homogeneous structure or as a structure with an impermeable core. It is judged that simulation with a core of equal permeability as the armour layer is more correct than applying an impermeable core. Therefore, modelling as a homogeneous structure has been applied. The friction factor, depending on the roughness of the surface and the flow characteristics, was derived by using the empirical formula of Madsen and White (1975), see also section 5.2. The depth in front of the structure d_s was 0.79 m. For the characteristic size of the armour unit, the $D_{n50}=0.034$ m was taken. The run-up is

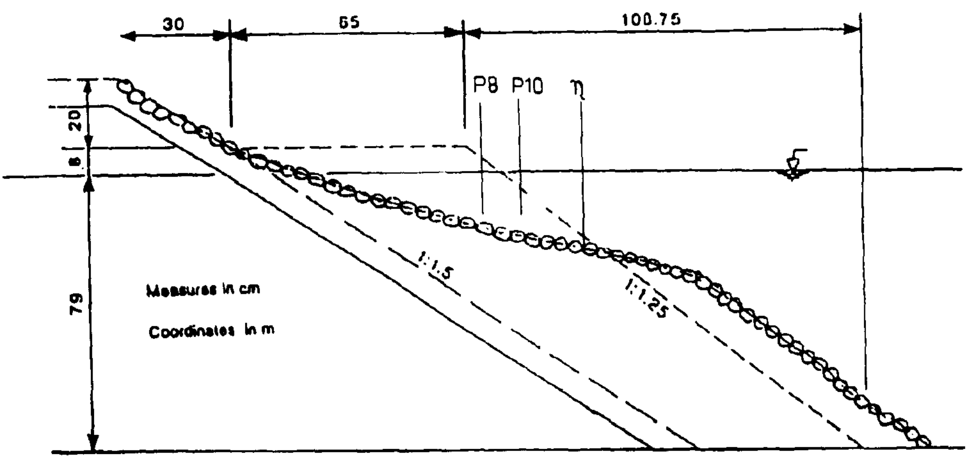

Fig. 8. Profile of the berm breakwater in the flume of N.H.L.-Trondheim.

about equal to the wave height for which 0.175 was used. For the angle of the slope, the angle from the berm section was taken ($\cot\alpha = 5$). This gives a friction factor $f = 0.15$. For the porosity, 0.35 was used. Added mass was not included because not enough measurements were performed yet to derive accurate added-mass coefficients. Including this added-mass, with a large uncertainty in the added-mass coefficient, would not necessarily lead to more accurate results. Both linear- and quadratic porous friction coefficients were included. A relatively large number of measurements, although only with stationary flow, have been performed to derive these coefficients so those values can be estimated much better than the added-mass coefficient.

Surface elevations were measured above the berm and a comparison with computed surface elevations has been done. The simulated wave conditions were the nine combinations of wave periods of 1.5, 1.8 and 2.1 s and wave heights of about 0.10, 0.15 and 0.20 m, see Table 1. The results of the comparisons of measured surface elevations with output from

Table 1
Combinations of wave periods and wave heights for comparison

1: $T = 1.5$ s; $H = 0.117$ m	4: $T = 1.8$ s: $H = 0.097$ m	7: $T = 2.1$ s; $H = 0.099$ m
2: $T = 1.5$ s; $H = 0.150$ m	5: $T = 1.8$ s; $H = 0.140$ m	8: $T = 2.1$ s; $H = 0.142$ m
3: $T = 1.5$ s; $H = 0.208$ m	6: $T = 1.8$ s; $H = 0.198$ m	9: $T = 2.1$ s; $H = 0.195$ m

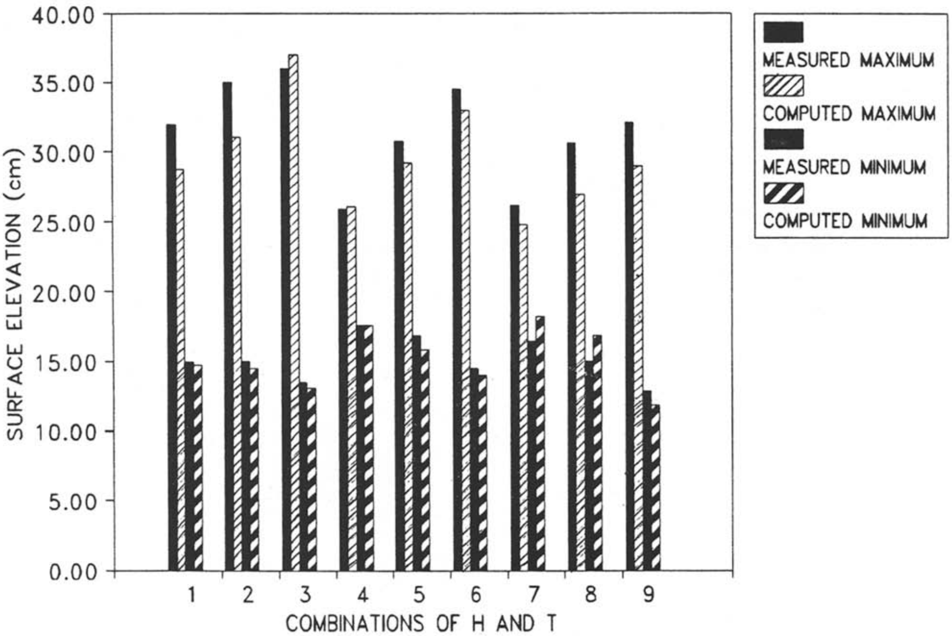

Fig. 9. Comparison of measured and computed surface elevations for nine combinations of wave period and wave height.

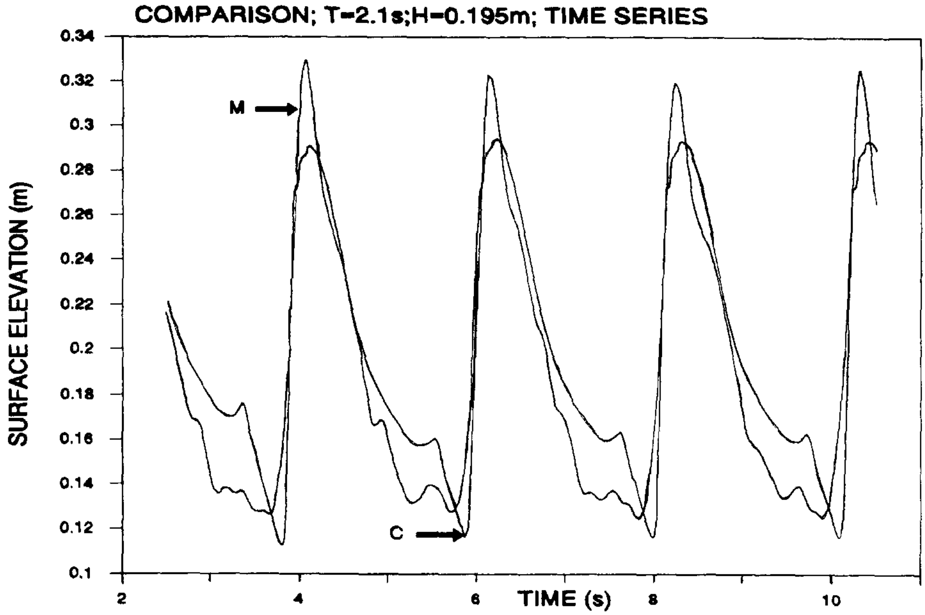

Fig. 10. Comparison between the measured (M) and the computed (C) surface elevations.

the numerical model, are summarized in Fig. 9. The values of the surface elevations are related to the local slope elevations.

The differences between the measured and the computed surface elevations show that the model underestimates the surface elevations. The average is 12.6% (about 0.02 m). This is the average value of the maximum minus the minimum surface elevations. This was done to exclude the influence of the difference between the assumed water depth (0.79 m) and the actual water depth. The wave condition $T=2.1$ s and $H=0.195$ m (combination 9) gives a difference (10.9%) in the same order of magnitude as the average difference (12.6%). Therefore this computation is supposed to give a representative impression of the differences. See Fig. 10. This figure shows local maxima both in the measured time-series and in the computed time-series. These local maxima are probably caused by reflected waves. The figure shows clearly that the absolute maxima are underestimated. In general, it can be concluded that the numerical model underestimates the surface elevations although the differences might be acceptable for many practical purposes.

7. Verification of velocities

For the verification of velocities, the measurements described in the previous section were used. Comparing the calculated depth-averaged velocities with the measured velocities in a certain point might be inappropriate. However, an approximation of the maximum boundary layer thickness gives 0.01–0.015 m, see Tørum (1991). This is rather low compared to the local water depth. Measured velocities in points above the boundary layer are assumed to be representative for the depth-averaged velocities. Measured velocities in different points above the slope, but in the same cross section, show differences in the order of magnitude of 20%. For comparisons, two measuring points have been selected. The velocities measured in point 8 and 10 (see Fig. 8), both above the berm and about 0.1 m away from each other, were used. Point 8 was positioned very close to the bottom and point 10 was about 0.07 m above the slope. Measuring-point 8 is about at the level of the estimated boundary thickness for these wave conditions. Point 10 is assumed to be above the boundary layer.

The comparison of simulated depth-averaged velocities with the measured (point) velocities are summarized in Figs. 11 and 12. Two measurements (combination 1 and 2) in point 8 were not carried out. The comparison shows that the numerical model underestimates the velocities with an average of 15.3% regarding the sum of the maximum uprush-velocity and the maximum downrush-velocity ($|U_{max} - U_{min}|$). All seven combinations give an underestimation. This is not fully due to the differences between the measured velocities at various positions in one cross-section. These differences were about 20%. Differences for point 8 do also appear because this point is so close to the bottom that the influence of the boundary layer is present here. Due to the overshoot effect this may lead to larger velocities in the boundary layer compared to the depth-averaged velocities. The velocities in the direction to the crest of the breakwater (U_{max}) show an average underestimation of 18.4%. For the velocities in the opposite direction (U_{min}) this underestimation is 8.4%.

Comparisons with data from measuring point 10 gave better results than for point 8. This

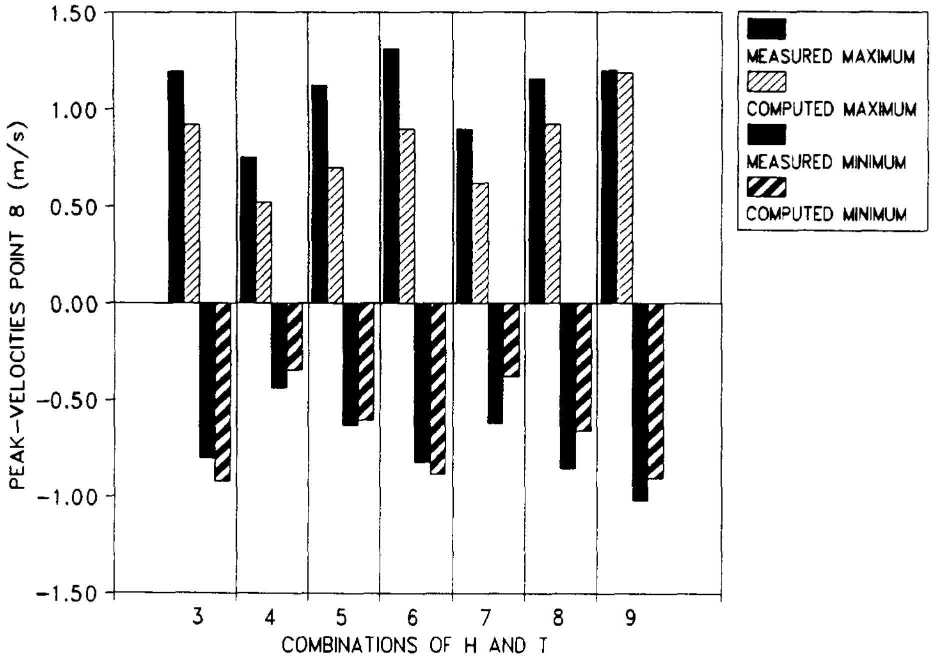

Fig. 11. Comparison of measured and computed velocities in point 8.

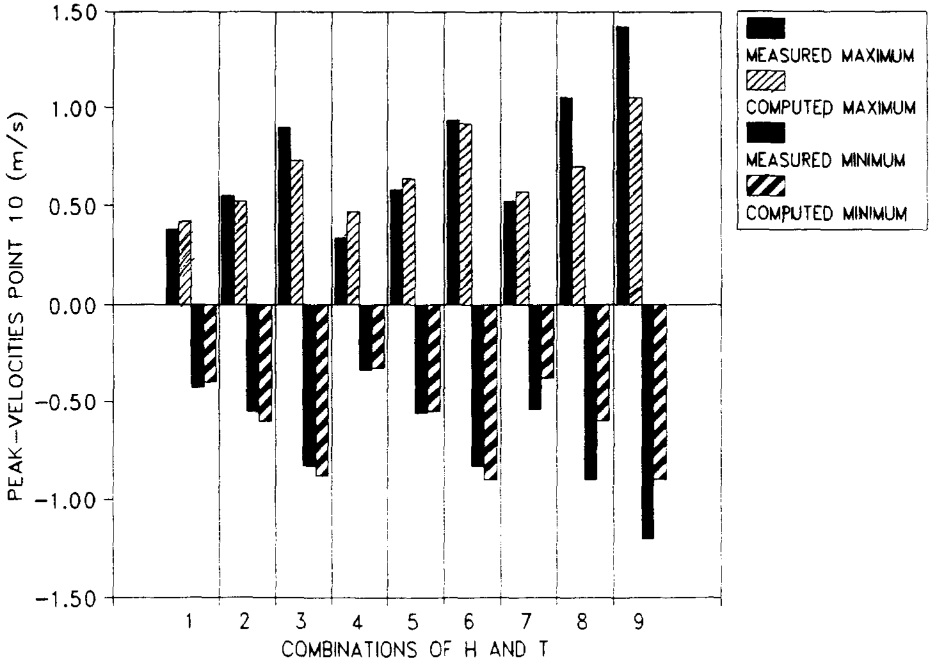

Fig. 12. Comparison of measured and computed velocities in point 10.

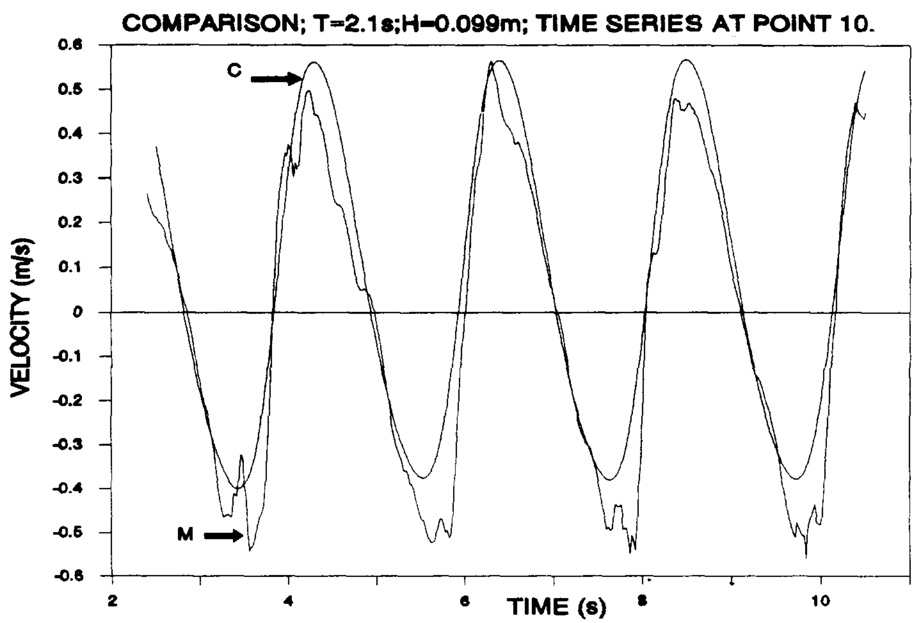

Fig. 13. Comparison between the measured (M) and the computed (C) velocities.

was to be expected because this measuring point 10 is not so close to the bottom as measuring point 8, so less influence of a boundary layer occurs. The average underestimation is now 5% ($|U_{max} - U_{min}|$); 1.2% towards the crest and 8.5% away from the crest.

Fig. 12 shows that the underestimation is relatively high for the combinations with high wave heights and long wave periods. For these cases, the boundary layer is relatively thick. Differences up to 35% occurred sometimes. In these cases, measuring point 10 may be influenced by the higher velocities of the boundary layer. Another explanation may be that for these combinations 8 and 9 with less steeper waves, breaking appears at a different position than for the other combinations with steeper waves. Breaking may appear close to the measuring position 10 for these two waves. At the position where the waves break, non of the point measurements will be representative for the depth-averaged velocity; the velocities differ too much over the cross-section. A comparison of point measurements with computed depth-averaged velocities in a cross section where the waves break, might be inappropriate. In section 6, the underestimated surface elevations have been discussed. If the surface elevations are underestimated, it seems reasonable that the velocities are underestimated as well.

Fig. 13 shows the comparison for a wave height of 0.099 m and a wave period of 2.1 s (combination 7) in measuring point 10. This combination gives a difference with the measurement of 10.4% which is a difference that is representative for the nine combinations. In general, the results show a fair agreement between the predicted velocities and the measured velocities although sometimes rather large difference occurred. Those differences are certainly not only due to the numerical modelling but also due to the fact that the comparison is done between point measurements (varying velocities in one cross-section) and depth-averaged velocities.

8. Sensitivity analysis

The numerical model contains several parameters that have to be prescribed. Although for each parameter recommended values are available, a sensitivity analysis is performed to study the influence of these parameters on the computed results. Each parameter was varied while the other parameters were kept the same. The sensitivity analysis has been performed for the peak-velocities in two positions above the most gentle sloping part of the berm of a berm breakwater. Results for the internal (U_p) and external velocities (U_h) for the two positions above the slope differ, but follow the same trends. Therefore only the velocities at one position will be discussed. The berm breakwater is similar as the one used for measurements at the Norwegian Hydrotechnical Laboratory in Trondheim (see Fig. 8). The breakwater was modelled as a homogeneous structure. The peak-velocities in the direction away from the structure are called U-min. All results described here, are done with a wave height of 0.175 m and a wave period of 1.8 s.

Fig. 14A shows that results with increased values of the roughness of the slope, described by the parameter f, show decreasing external velocities and increasing internal velocities. The porosity n (see Fig. 14B) was varied between 0 (impermeable) and 0.9 although the relevant range is between 0.35 and 0.5. The internal velocities increase with increasing porosity as one would expect. The maximum external velocities in the direction away from

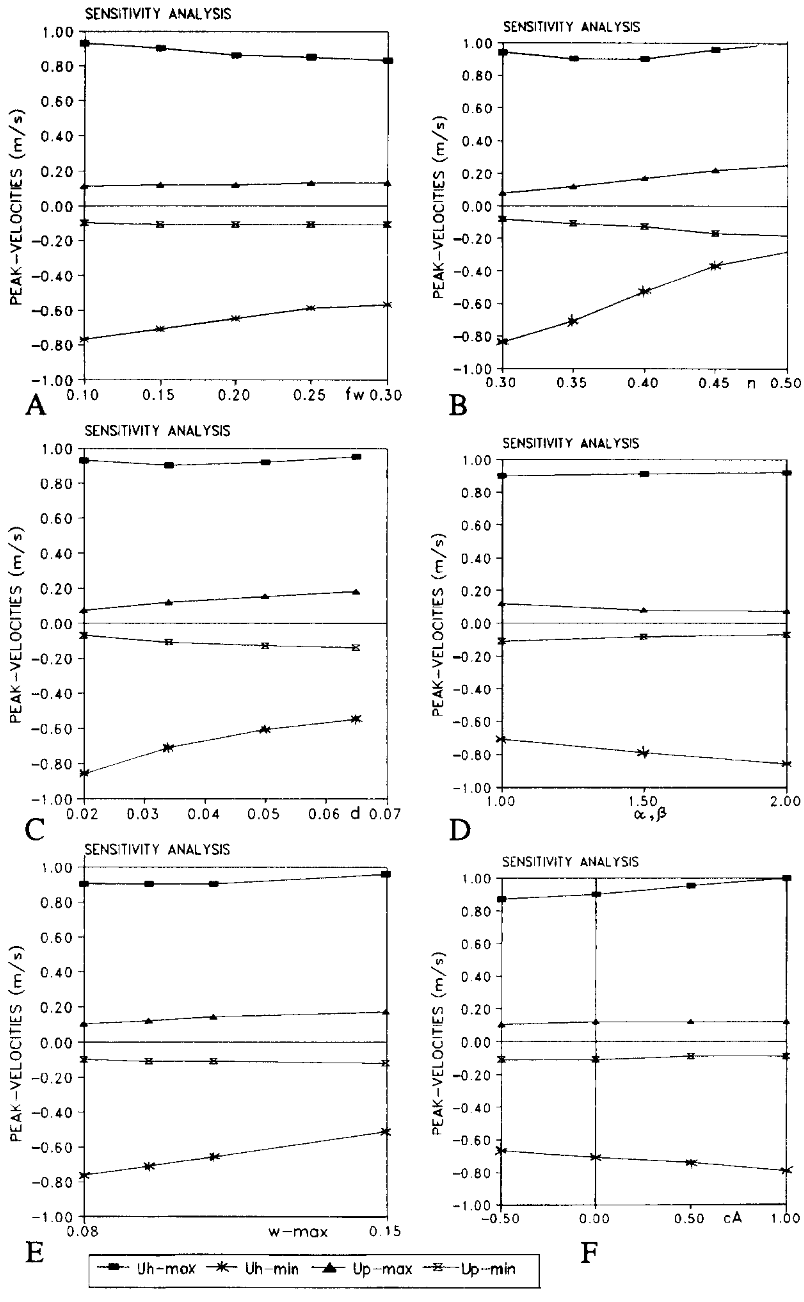

Fig. 14. Sensitivity analysis; variation of the peak velocities with variation of several parameters.

the structure, decrease with increasing porosity. The net flow through the structure increases as one would expect with a more open structure.

The diameters of the stones have influence on the Forchheimer friction terms. Larger stones give less resistance in the porous part. The model shows that larger stones give lower external velocities away from the structure (see Fig. 14C). This gives a larger net flow through the structure. One would expect this if the structure gives less resistance. The friction coefficient f may increase due to larger stone diameters. This is not taken into account.

The coefficients a and b from the Forchheimer friction terms, describe the resistance of the porous medium ($I=a\cdot u+b\cdot u|u|$). The coefficients are written as $a=\alpha\cdot(1-n)^2/n^3\cdot \nu/(gD^2)$ and $b=\beta\cdot(1-n)/n^3\cdot 1/(gD)$. Values computed from measurements by Shih (1990), were used for the coefficients α and β. They were both increased with factors 1.5 and 2. Results with increased α and β, show a similar trend as results with decreased stone diameters, as one would expect (see Fig. 14D). The values of α and β were increased with a factor 1.5 because this may lead to better results: The model does not take the resistance in the vertical direction into account, except for limited in- and outflow velocities. Assuming that the average direction of the velocity has an angle of 45°, increasing the resistance in the x-direction with a factor $\sqrt{2}$ (≈ 1.5), may lead to better results. The real values of the coefficients α and β are not exactly known till now although recently many measurements have been carried out.

The fluctuation of the phreatic level (related to the maximum value of the vertical velocity, w-max) has a maximum and this is treated in the model as described in Van Gent (1992b). In this case, the recommended value for w-max is 0.095 m/s (see also Fig. 14E). If one neglects this phenomenon ($w\text{-max}=\infty$), much different results will be obtained compared with results with $w\text{-max}=0.095$. In this case, the velocities towards the structure increase with 20% and the velocities in the opposite direction decrease with about 40%. The internal velocities increase also quite a lot. This shows that the structure seems much more permeable if this phenomenon is not taken into account. The maximum rising of the phreatic level may be less influenced by this phenomenon than the maximum drop of the phreatic level. Therefore, for the maximum value for rising, a value twice (0.190 m/s) the one for a drop of the phreatic level (0.095 m/s) has been used in one of the computations. This gave very similar results as for the recommended value $w\text{-max}=0.095$ m/s in both directions. The assumption that the mentioned maximum change of the phreatic level is the same in both directions, seems not to be very important in this case; the results do not differ so much comparing with the results of the computation with an increased maximum upward-velocity.

The flow between the hydraulic part and the porous part has a maximum as well. This is implemented assuming a maximum pressure gradient in the vertical direction. This pressure gradient is assumed to be 1 but can be changed with the coefficient c_F (with 1 as the recommended value), see Van Gent (1992b). Not taking this phenomenon into account gives again very different results. The velocities at the regarded positions are much higher if this phenomenon is not taken into account. Results differ up to 20% for the external velocities and up to 70% for the internal velocities. Computations showed that in this case, limiting the outflow seems to be more important than limiting the inflow.

Finally the coefficient for added mass c_A has been studied. It was found that the influence of this added mass, which is of course only present in the porous part, has an effect on the external velocities that can not be neglected if the c_A values are near the value one (see Fig. 14F). It seems to be important to do further study to find the exact values for c_A.

The sensitivity analysis shows that all variations of the velocities, due to variations of the parameters, can be explained. The conclusion can be drawn that those phenomena are reproduced in a qualitative way. In the previous sections it was already verified, to some extend, whether flow-properties are reproduced well in a quantitative way.

9. Comparing impermeable and permeable structures

A comparison is made between the wave action, described by the model, on an impermeable breakwater, a permeable (homogeneous) berm breakwater and a permeable berm breakwater with an impermeable core. The profile as shown in Fig. 8, has been used. A comparison between the results for impermeable and permeable structures is useful to show whether results differ or not. If so, the description of the porous flow is of importance to describe the external flow as well.

Computations were done for a slope divided in 7 slope sections. The friction coefficient f was estimated using the formula from Madsen and White (1975) for fully turbulent flow on a uniform sloping breakwater ($f=0.15$). The wave height was 0.20 m, the wave period was 1.5 s and the still water-level was set at 0.80 m. The value of Δ for the minimum water depth in the hydraulic model during the computation was set at 0.005 m, see also Fig. 1. The space-step was taken 0.015 m. Thousand time-steps per wave period were computed. Higher values of the space-step and time-step are possible without instability of the computation process but with decreasing accuracy. In case porous flow was included a porosity of 0.4 and an equivalent diameter of the stones of 0.035 m, were prescribed. Added mass was not included because not enough measurements were performed yet to derive accurate added-mass coefficients. Both linear- and quadratic porous friction coefficients were included. For the coefficients α and β (see Eq. 3), the values 2120 and 2.0 have been used.

Fig. 15 shows the surface elevations at ten points of time within one wave cycle for the permeable berm breakwater with an impermeable core. The extreme velocities that occurred within one wave cycle are shown in Fig. 16. The positive values are in the direction of the crest of the structures. Transmission through the homogeneous structure gives considerably lower velocities away from the structure. The maximum and minimum surface elevations for both structures are shown in Fig. 17. Above the berm the wave heights are lower for the permeable structures. Reflection caused by down-rushing water causes an increase of the maximum wave height in this area for the impermeable structure. This influence is much weaker for a permeable structure.

Fig. 17 shows that the run-up levels are much lower for the permeable structures. Fig. 18 shows these levels as a function of time. The infiltration and a less intensive wave action diminish the run-up.

Fig. 19 shows the velocity of the wave front as a function of time. This wave front is computed by taking the average of the velocities of the three most upper computation-points containing water. The maximum velocities in the direction of the crest of the structure, are much higher than in the opposite direction. The maxima do not differ a lot although they

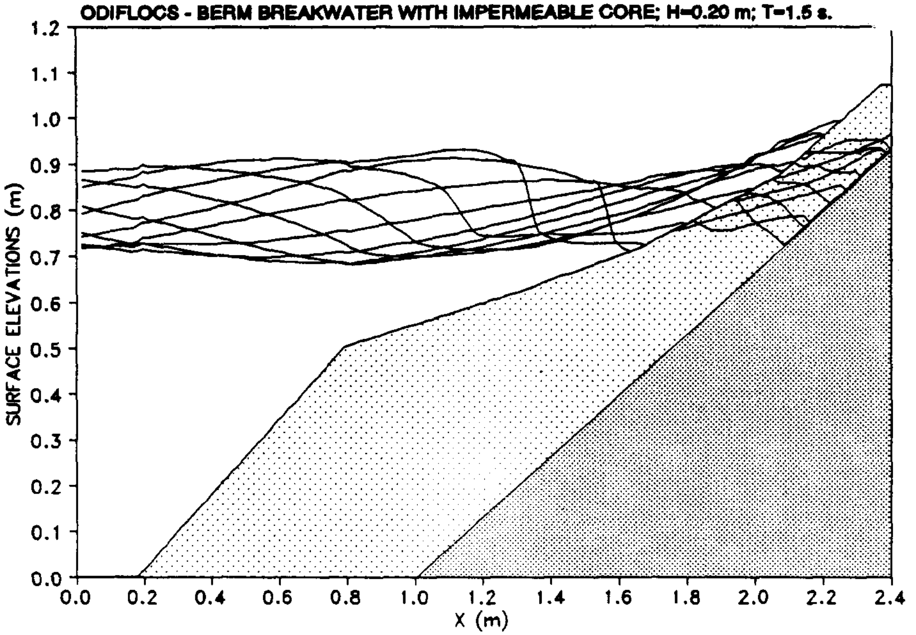

Fig. 15. Surface elevations at ten point of time during one wave cycle for a berm breakwater with an impermeable core.

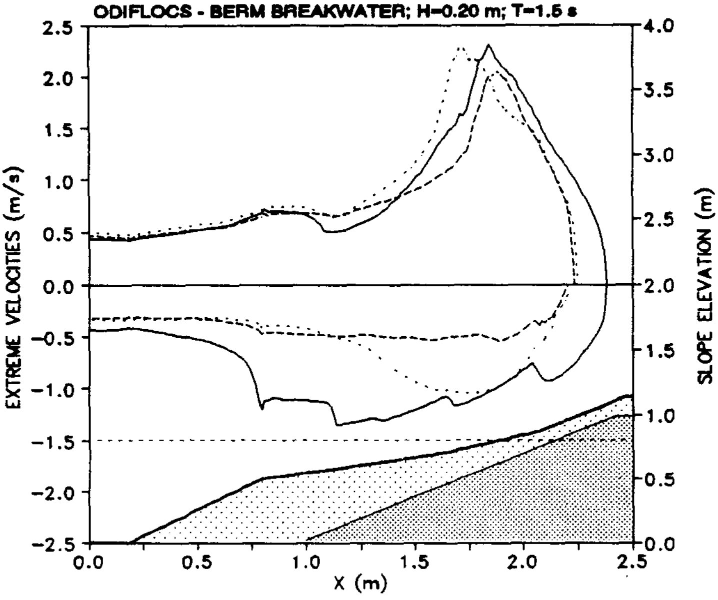

Fig. 16. Extreme velocities that occurred within one wave cycle.

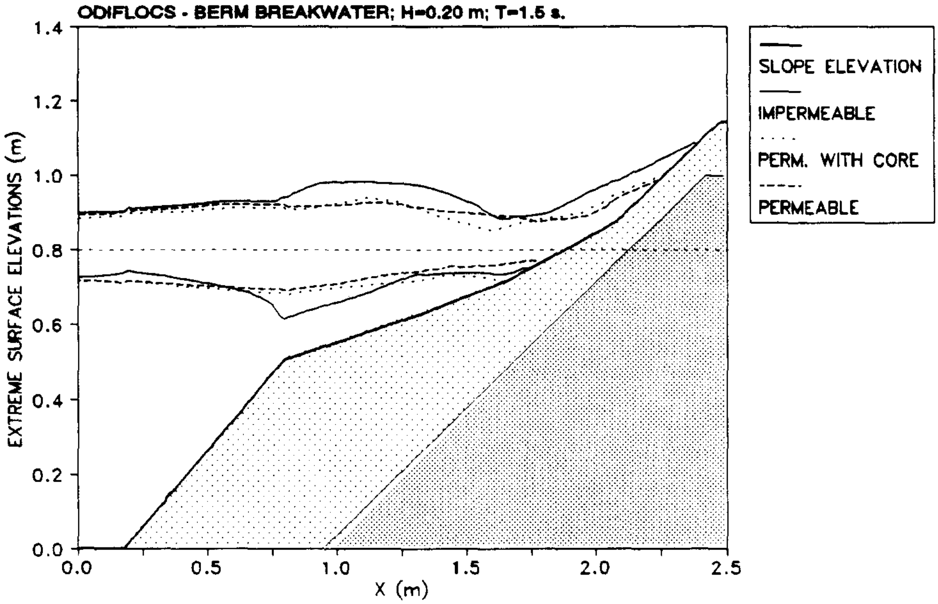

Fig. 17. Extreme surface elevations that occurred within one wave cycle.

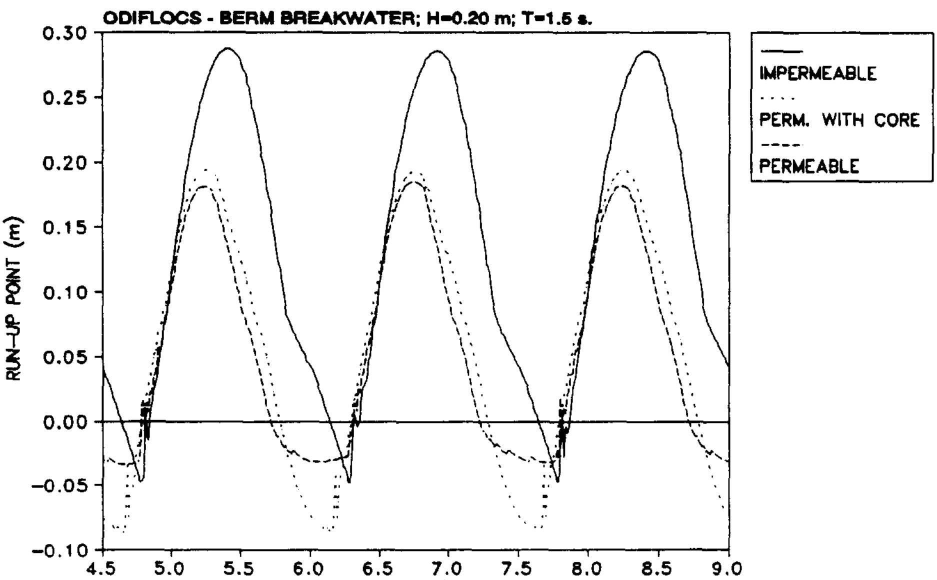

Fig. 18. Run-up point as a function of time.

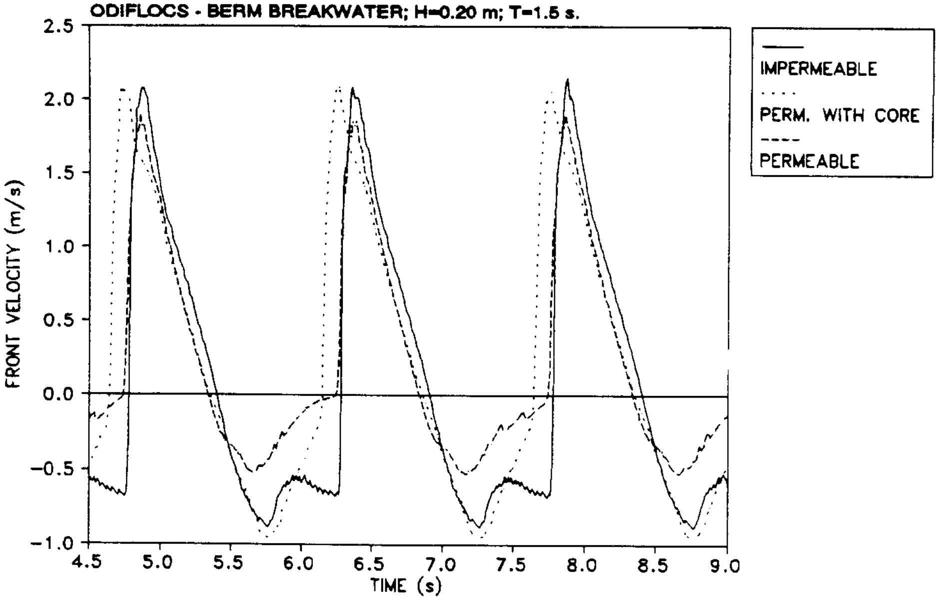

Fig. 19. Front velocities as a function of time.

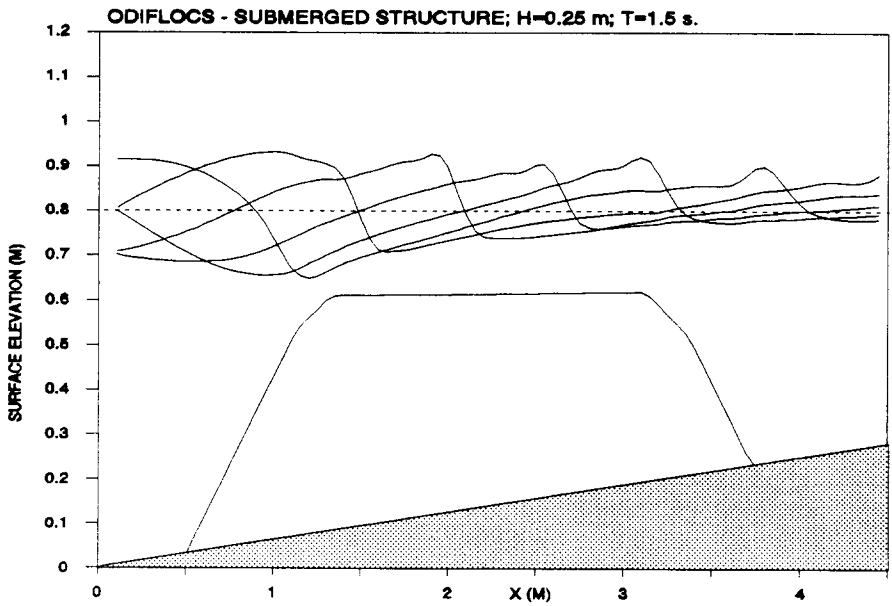

Fig. 20. Surface elevations at five points of time.

occur at different positions. The peak velocities are the highest in the direction away from the structure.

The results described above show that a description of the porous flow is not only necessary to describe the porous flow itself but that it has an important influence on the external flow as well. This shows the necessity of an integrated model describing the external flow, the internal flow and a coupling between those.

10. Application with submerged structures

A computation for a permeable submerged structure is done. It shows that the model can compute overtopping and that the non-reflecting boundary at the "landward" side works. Whether the model gives also valuable results for submerged structures must be verified. For the computation a friction coefficient $f=0.15$ was taken just like in the computations described in the previous section. The wave height was 0.25 m, the wave period was 1.5 s and the still water-level was set at 0.80 m. The space-step was taken 0.05 m. For the time-step 0.005 s was used. A porosity of 0.4 and an equivalent diameter of the stones of 0.035 m, were prescribed. Again added mass was not included. Both linear- and quadratic porous friction coefficients were included. Fig. 20 shows the surface elevation at five points of time as a function of place. The shape of the structure is plotted as well. The structure is situated on an impermeable sloping bottom.

11. Application with internal set-up

Internal set-up is a phenomenon that is closely related to an accurate description of the disconnection of the free surface and the phreatic surface. Therefore, study on this phenomenon has been done. The average phreatic level in a permeable structure increases if the structure is closed on the harbour side. The inflow during a wave period is dominating if the surface elevation outside the structure is high. The outflow is dominating if the free surface elevation is relatively low. The inflow of water occurs over a larger area than the outflow. This results in an average inflow that will finally be counteracted by a sloping phreatic level. See Barends (1984).

Three computations have been done to verify whether the model predicts any internal set-up. As described by Hölscher et al. (1988), a filter had to be constructed for the breakwater of the harbour of Zeebrugge. A new port area was planned behind the breakwater by constructing a sand backfill. This sand backfill is modelled as being impermeable. For the construction of the filter between the core of the breakwater and the sand backfill, internal set-up had to be studied. Set-up may have caused inundation of the port area. This possible inundation has been verified with the model. Similar computations have been done with ODIFLOCS as done by Hölscher et al. (1988). The structure was schematized as a homogeneous structure where for the size of the stones, the diameter of the core material was used. A storm was characterized by a regular wave of 6.5 m high and a period of 9 s. The depth in front of the breakwater was 11 m (storm surge level).

Computations were done with a porosity of 0.3 (rather low) and a stone diameter of 0.2

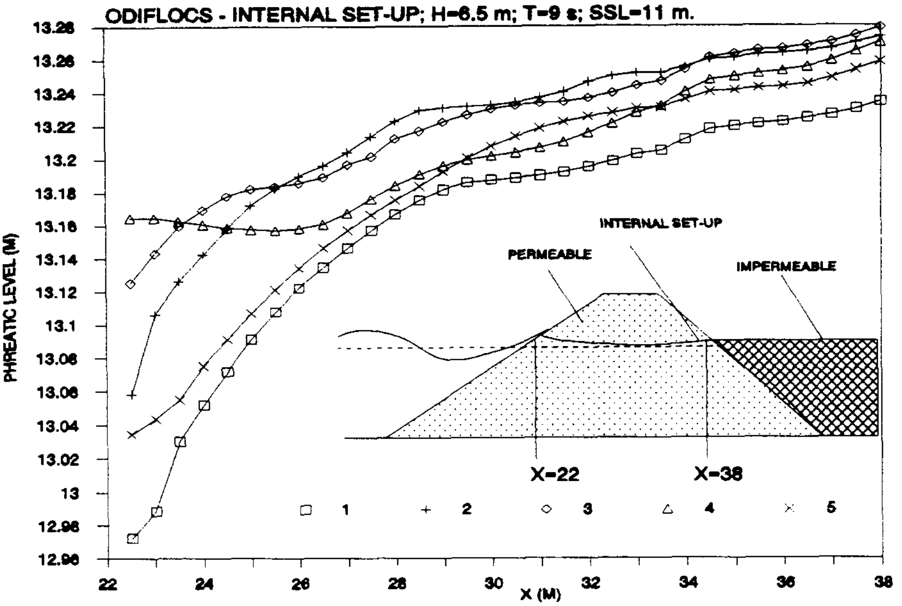

Fig. 21. The phreatic level at five points of time within one wave cycle. The left-hand side is the open side of the structure, the right hand side is closed.

m. The coefficients α and β from the Forchheimer friction terms were varied to show the influence of the friction of the porous medium with respect to internal set-up. The calculated internal set-up at the back of the structure was 0.82 m, using values for α and β proposed by Shih (1990). The calculated internal set-up with values of α and β twice the proposed values, was 1.81 m. Values three times the proposed values gave a set-up of 2.17 m. For this last computation the phreatic levels at five points of time during one wave cycle are shown in Fig. 21. Results show a clear dependency on the friction terms. Because those porous friction terms are not exactly known, no conclusions concerning inundation will be made. The third computation with very large friction terms and a rather low porosity provides a set-up level that is probably higher than the one occurring in reality. Therefore, the port area will probably not be inundated if its level is 2 m above the storm surge level. Research concerning the exact values of α and β is desirable. The conclusion is that the model ODIFLOCS simulates internal set-up and that the set-up increases with decreasing permeability, which is correct.

12. Prediction of the permeability of a structure

The stability formulae of Van der Meer have proved to be accurate for prediction of armour layer stability. To estimate this stability, the empirical permeability coefficient P is one of the parameters to be prescribed. This permeability coefficient P is set at 0.6 for homogeneous structures and 0.1 for structures with an impermeable core. Using the extensive model investigation, the permeability coefficient P was set at 0.5 for structures with a permeable core wherein the size of the core material is $D_{n50}(\text{core}) = D_{n50}(\text{armour})/3.2$. For estimation of the coefficient P for other structures, test results can be used. Hölscher et al. (1988) and Van der Meer (1988) used the numerical model HADEER for a relation between the coefficient P and hydraulic properties of the core. A relation between P and the rate of inflow was found. The model ODIFLOCS can also give such a relation.

The total volume of water that flows into the structure during one wave cycle (Q_0) was computed. The flow was simulated for three structures. First a homogeneous structure was computed where for the stones the size of the armour stones was used ($D_{n50} = 0.25$ m). After that, a homogeneous structure was computed where for the size of the stones, $D_{n50} = 0.08$ m was taken. This size gives the rate $D_{n50}(\text{armour})/D_{n50}(\text{core}) = 3.2$ for which $P = 0.5$ is defined. The third computation was done with a homogeneous structure using the stone size of the actual core, for which one wants to compute the P coefficient. For this third size $D_{n50} = 0.05$ was used. The slope of the structure was 1:3. A wave height of 1 m was used with wave periods of 3.5, 4.5 and 7.0 s resulting in surf similarity parameters of $\xi = 2.9$, 1.9 and 1.5. The friction coefficient f was computed with the formula of Madsen and White (see section 2.2) which gave $f = 0.17$. In all computations for the porosity n was taken as 0.35.

The first computation, with the material of the armour layer, gives the total volume of water that flows into the structure (Q_0). This gives $P = 0.6$. The second computation gives a volume Q. The rate Q/Q_0 was 0.63, 0.83 and 0.65 for respectively $T = 3.5$, $T = 4.5$ and $T = 7$ s. These values give $P = 0.5$. For impermeable structures $P = 0.1$ is prescribed. This gives a curve through three points for each value of ξ, see Fig. 22. In this figure, two lines $\xi = 2.9$ and $\xi = 1.5$ are the same. The third computation gave a rate $Q/Q_0 = 0.50$, 0.67 and 0.52 for respectively $T = 3.5$, $T = 4.5$ and $T = 7$ s. For this third structure, the P coefficient is unknown. Starting from the y-axis horizontally to the curve and vertically from the curve to the x-axis, gives the P coefficient for that particular structure. This procedure gives $P = 0.44$ for $\xi = 1.9$ and $P = 0.47$ for $\xi = 2.9$ and $\xi = 1.5$, so the P coefficient is about 0.44 to 0.47. The computations with the porous flow model HADEER, using measurements at the slope as an input signal, (see Van der Meer, 1988) gave $P = 0.42$ to 0.44. The conclusion

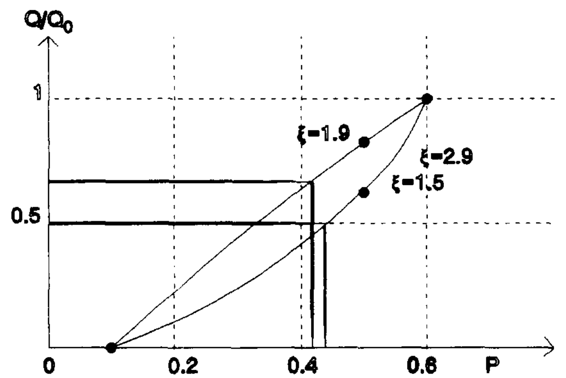

Fig. 22. Relation between volume of inflow and the permeability coefficient P.

is that the model ODIFLOCS can be used to predict the permeability coefficient P without measurements. Therefore, the model can, in combination with other tools, also be applied for the determination of stability of rock slopes.

13. Approach to derive a 2-D impression of the flow field

13.1. Approach to derive velocity vectors

Because the model uses depth-averaged velocities, no vertical velocities are computed directly. This does not mean that no estimation concerning these vertical velocities can be given. The slope of the surface elevation, the slope of the bottom elevation, the variation of the surface elevation in time, and the flow q through the boundary between hydraulic and porous part, contain information that can be used for calculation of vertical components of the velocity vectors. Because of the number of assumptions that have to be made and the limited accuracy of a one-dimensional model in the first place, the calculated vertical components probably differ from reality. However, they may still give a rough impression of the velocity field. This interpretation has no influence on the computation in the model

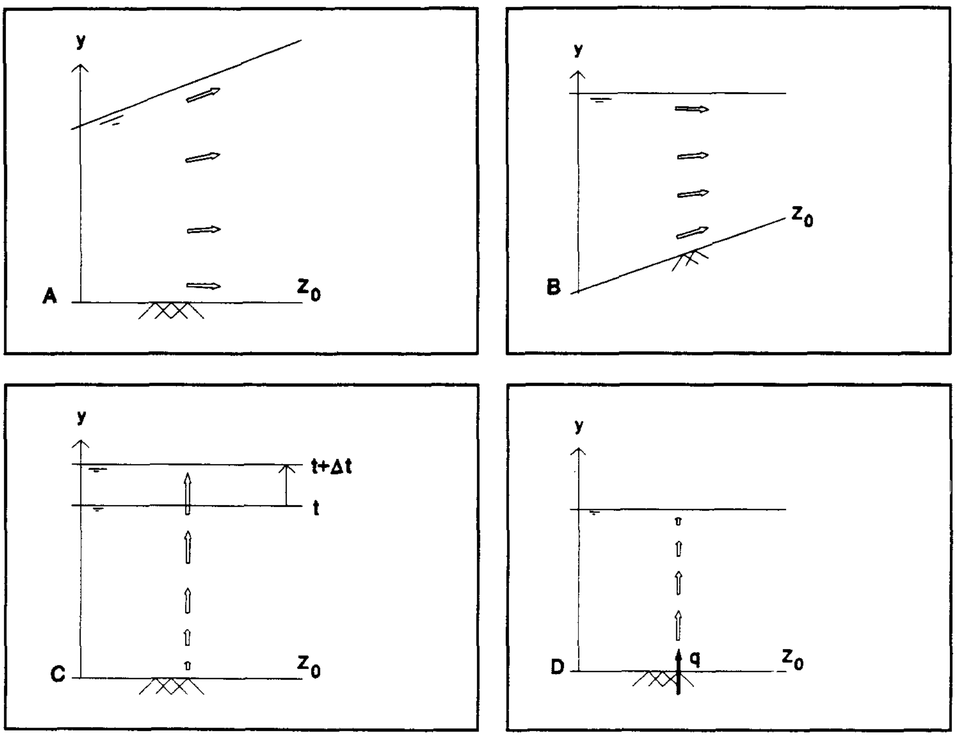

Fig. 23. Four contributions to the vertical component of the velocity vectors.

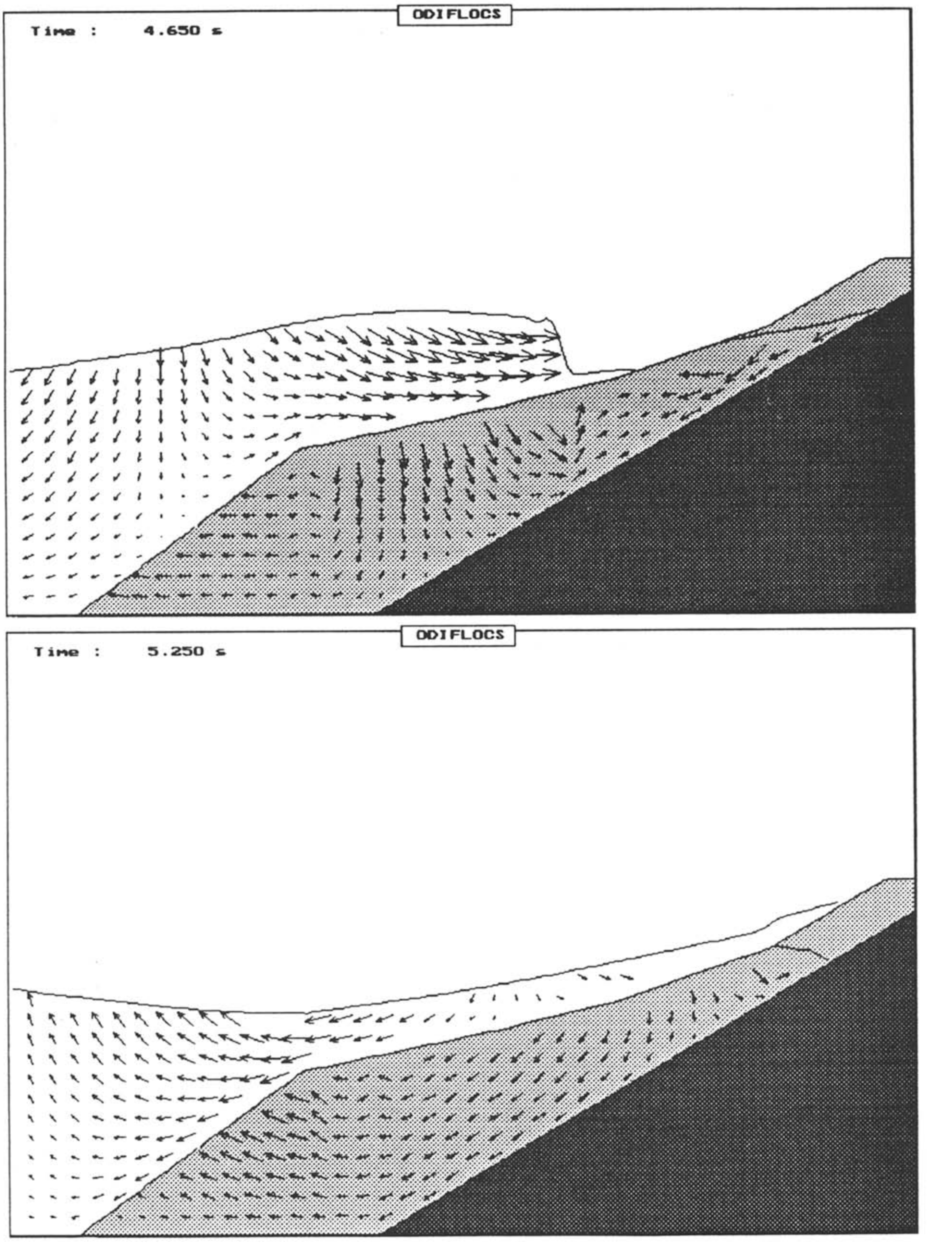

Fig. 24. Impressions of the flow field for a berm breakwater.

itself. A description of how velocity vectors are calculated from output of the model will be discussed below.

The depth-averaged horizontal velocities computed by the model from the differential

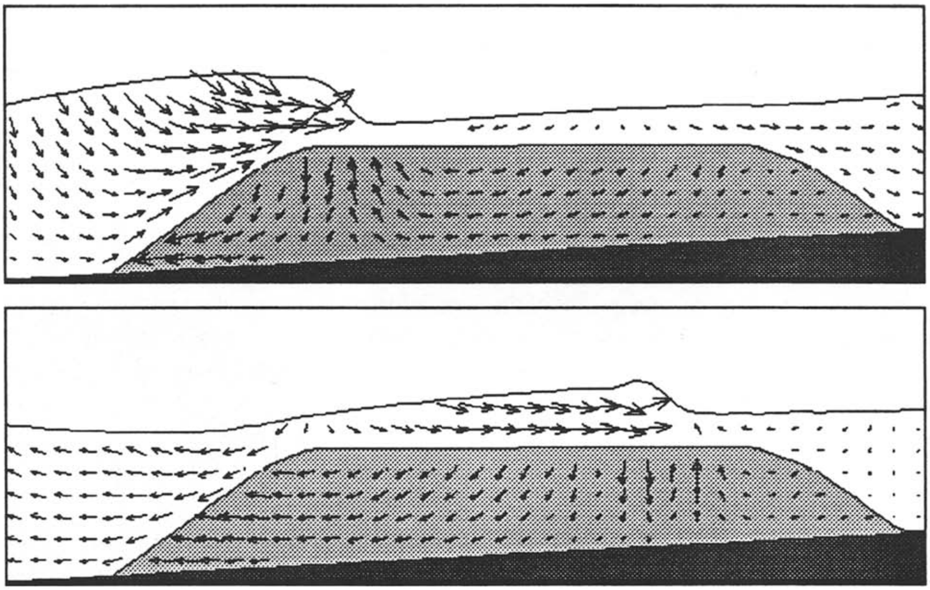

Fig. 25. Impressions of the flow field for a submerged structure.

equations are assumed to be the horizontal components of the velocity vectors in each position above the slope. This is of course not true because in reality the distribution of the horizontal velocities in the vertical is influenced by for instance the bottom friction and the breaking of a wave. Because results of the model do not contain information concerning this distribution, the horizontal components are the same at each position above the slope except for the influence of the flow q. This will be explained later.

Four contributions to the vertical components of the velocity are shown in Fig. 23. The slope of the free surface, the slope of the structure, the mutation of the surface in time, and the interactive flow q give contributions to the vertical components of the velocity vectors. The sum of these four components give the vertical components of the vectors. The four contributions are all derived using the assumption of a linear distribution over the water depth. The contribution of the slope of the free surface (Fig. 23A) can be expressed as: $u_y = u_{d\text{-}a} \Delta h / \Delta x \, (y - z_0)/h$ where $u_{d\text{-}a}$ is the depth-averaged horizontal velocity and z_0 the slope elevation. The contribution of the slope of the bottom elevation (Fig. 23B) can be expressed as: $u_y = u_{d\text{-}a} \Delta z_0 / \Delta x (1 - (y - z_0)/h))$. The third contribution (Fig. 23C) is caused by the variation of the surface elevation in time: $u_y = \Delta h / \Delta t (y - z_0)/h$. The flow q between the hydraulic model and the porous flow model causes the fourth contribution: $u_y = (\cos\alpha)^2 (1 - (y - z_0)/h) q$. This flow q is assumed to be perpendicular to the slope. In case the slope of the bottom is horizontal, Fig. 23D is valid.

The flow q has also a component in the x-direction if the slope is not horizontal: $u_x = -\cos\alpha \sin\alpha (1 - (y - z_0)/h) q$. Again a linear distribution over the depth with its maximum at the slope and a zero contribution at the free surface has been assumed. Together with the depth-averaged velocity this gives the x-components of the vectors. For the vectors inside the structure a similar approach has been used.

13.2. Impressions of the flow field

Some applications of the approach described in the previous section are shown in Fig. 24, giving impressions of the flow field. A similar computation for a berm breakwater as shown in Fig. 8 has been used. An impermeable core is implemented. The scale for the vectors inside the breakwater is taken three times larger than for the vectors outside the breakwater. Fig. 25 gives impressions of the flow field for the computation with a submerged structure as described in section 10. Again the scale for the velocity vectors inside the structure is taken three times larger as for the vectors of the external flow.

14. Conclusions

A set of long wave equations is used for a numerical model in which the flow on the structure is described with a hydraulic model and the flow in the structure is described with a porous flow model. The coupling of those two parts resulted in an integrated model containing descriptions of many phenomena. In the model, the free surface and the phreatic surface do not have to be connected. This is an important aspect for a combined external–internal flow description. The model contains also infiltration, seepage and overtopping. The numerical model gives satisfactory results for conventional- and berm breakwaters. Comparisons with measurements of run-up and run-down levels show that the model can compute run-up levels for smooth impermeable structures and permeable structures, rather accurate. Run-down levels differ more and can only be used within the limited range $2 < \xi_0 < 3$. Comparisons with measured surface elevations and measured velocities above a berm breakwater slope give a fair agreement as well. The sensitivity analysis shows that the variations of the velocities, due to variations of the parameters of the numerical model, follow trends that one would expect. The numerical model simulates internal set-up in cases in which one would expect it to appear. A smaller permeability gives a larger internal set-up. The disconnection of the phreatic surface and the free surface, seems to work properly. The model can estimate the permeability coefficient P from the stability formulae from Van der Meer without use of measurements. In general, one can conclude that the results described in this paper, show that the model ODIFLOCS is a useful engineering tool. However, verification is necessary for applications on situations that have not been verified till now. Research concerning the determination of the porous friction coefficients may lead to further improvements of the model.

Acknowledgements

This study is co-sponsored by the Commission of the European Communities within the framework of the MAST-G6S project (contract 0032-C). I would like to express my appreciation to all partners in this MAST group for using of the numerical model and giving their comments, in particular to Dr. J.W. van der Meer and Mr. H.A.H. Petit from Delft Hydraulics, Prof. A. Lamberti from the University of Bologna, and Prof. F.B.J. Barends from Delft Geotechnics. Special thanks are due to Prof. A. Tørum from N.H.L.-Trondheim who provided all the necessary data from measurements above a berm breakwater slope. Mr. M.Z. Voorendt (Delft University) has been of great help during the numerical modelling.

References

Ahrens, J.P., 1975. Large wave tank tests of riprap stability. Technical memorandum No. 5, U.S. Army, Corps of Engineers, CERC, Ft. Belvoir, VA, 22060.

Barends, F.B.J., 1984. Internal set-up in breakwaters. Report No. SE 680294, Delft Geotechnics.

Burger, A. and Van der Meer, J.W., 1983. Slope-protection of placed block-revetment, large-scale research in the Delta flume of placed block-revetment on sand (in Dutch). Report No. M1795/M1881, Part XII, Delft Hydraulics.

Hannoura, A.A. and Barends, F.B.J., 1981. Non-darcy flow; A state of the art. In: Proc. Euromech 143, Delft.

Hölscher, P., De Groot, M.B. and Van der Meer, J.W., 1988. Simulation of internal water movement in breakwaters. In: Kolkman et al. (Editors), Modelling Soil–Water–Structure Interactions. Balkema, Rotterdam, ISBN 906191 8154.

Kobayashi, N., Otta, A.K. and Roy, I., 1987. Wave reflection and run-up on rough slopes. J. Waterw. Port Coastal Ocean Eng. ASCE, 113(3).

Madsen, D.S. and White, S.M., 1975. Reflection and transition characteristics of porous rubble mound breakwaters, Report No. 207, R.M. Parsons Lab, Dept. of Civil Eng., Massachusetts Institute of Technology, Cambridge, Mass.

Shih, R.W.K., 1990. Permeability characteristics of rubble material, new formulae. In: Proc. ICCE'90, Delft, Vol. 2, pp. 1499–1512.

Tørum, A., 1992. Wave induced water particle velocities and forces on an armour unit on a berm breakwater. MAST-G6S report and Report No. STF 60-A92/04, NHL Trondheim.

Tørum, A. and Van Gent, M.R.A.. 1992. Water particle velocities on a berm breakwater. In: Proc. ICCE'92, Venice, Vol. 2, pp. 1651–1665.

Van der Meer, J.W., 1988. Rock slopes and gravel beaches under wave attack, Ph.D. thesis, Delft University of Technology and Delft Hydraulics.

Van der Meer, J.W. and Klein Breteler, M., 1990. Measurements and computation of wave induced velocities on a smooth slope. In: Proc. ICCE'90, Delft, Vol. 1, pp. 191–204.

Van Gent, M.R.A., 1992a. Formulae to describe porous flow. In: Communications on Hydraulic and Geotechnical Engineering, No. 92-2. ISSN 0169-6548, Delft University of Technology, Delft.

Van Gent, M.R.A., 1992b. Numerical Model for Wave Action on and in Coastal Structures. Communications on Hydraulic and Geotechnical Engineering, No. 92-6. ISSN 0169-6548, Delft University of Technology, Delft.